

Passive manipulation of free-surface instability by deformable solid bilayers

Shivam Sahu and V. Shankar*

Department of Chemical Engineering, Indian Institute of Technology, Kanpur 208016, India

(Received 18 May 2016; published 22 July 2016)

This study deals with the elasto-hydrodynamic coupling that occurs in the flow of a liquid layer down an inclined plane lined with a deformable solid bilayer and its consequences on the stability of the free surface of the liquid layer. The fluid is Newtonian and incompressible, while the linear elastic constitutive relation has been considered for the deformable solid bilayer, and the densities of the fluid and the two solids are kept equal. A temporal linear stability analysis is carried out for this coupled solid-fluid system. A long-wave asymptotic analysis is employed to obtain an analytical expression for the complex wavespeed in the low wave-number regime, and a numerical shooting method is used to solve the coupled set of governing differential equations in order to obtain the stability criterion for arbitrary values of the wave number. In a previous work on plane Couette flow past an elastic bilayer, Neelmegam *et al.* [*Phys. Rev. E* **90**, 043004 (2014)] showed that the instability of the flow can be significantly influenced by the nature of the solid layer, which is adjacent to the liquid layer. In stark contrast, for free-surface flow past a bilayer, our long-wave asymptotic analysis demonstrates that the stability of the free-surface mode is insensitive to the nature of the solid adjacent to the liquid layer. Instead, it is the effective shear modulus of the bilayer G_{eff} (given by $H/G_{\text{eff}} = H_1/G_1 + H_2/G_2$, where $H = H_1 + H_2$ is the total thickness of the solid bilayer, H_1 and H_2 are the thicknesses of the two solid layers, and G_1 and G_2 are the shear moduli of the two solid layers) that determines the stability of the free surface in the long-wave limit. We show that for a given Reynolds number, the free-surface instability is stabilized when G_{eff} decreases below a critical value. At finite wave numbers, our numerical solution indicates that additional instabilities at the free surface and the liquid-solid interface can be induced by wall deformability and inertia in the fluid and solid. Interestingly, the onset of these additional instabilities is sensitive to the relative placements of the two solid layers comprising the bilayer. We show that it is possible to delay the onset of these additional instabilities, while still suppressing the free-surface instability, by manipulating the ratio of the shear moduli and the thicknesses of the two solid layers in the bilayer. At moderate Reynolds number and finite wave number, we demonstrate that an exchange of modes occurs between the gas-liquid and liquid-solid interfacial modes as the solid bilayer becomes more deformable. We demonstrate further that dissipative effects in the individual solid layers have an important bearing on the stability of the system, and they could also be exploited in suppressing the instability. This study thus shows that the ability to passively manipulate and control interfacial instabilities increases substantially with the use of solid bilayers.

DOI: [10.1103/PhysRevE.94.013111](https://doi.org/10.1103/PhysRevE.94.013111)**I. INTRODUCTION**

Interfacial instabilities are often encountered in two-layer and multilayer flows of dissimilar liquids [1–3] due to discontinuity in physical properties such as viscosity or elasticity of the liquid layers across the interface. The origin of these instabilities can be elastic or viscous depending upon the viscoelastic [4,5] or Newtonian nature of the liquid layers [6–8] considered. In many practical settings, it is often desired to control and manipulate these instabilities at the interface. In some instances such as coating flows, instabilities are undesirable, while in some other applications such as drop formation using microfluidic flow-focusing [9,10], it is desirable to induce interfacial instabilities. There have been several earlier investigations that have explored “active” manipulation techniques such as imposed wall oscillations and heating of the substrate, with an objective toward suppressing the interfacial instabilities [8,11]. Recently, “passive” manipulation of these instabilities using deformable solid layers has been suggested [12–14] as a possible alternative. Passive

manipulation techniques have the potential to be of relevance to microfluidic applications and coating processes, wherein interfacial instabilities need to be induced or suppressed. In microfluidic devices made of the elastomer PDMS, it is possible to tune the shear modulus of the elastomer to manipulate and control the interfacial instability in a passive way. In the present work, we propose and evaluate a passive manipulation methodology that exploits the use of a deformable solid *bilayer*, and we study its impact on the stability of a liquid film flowing down an inclined plane lined with the bilayer. The onset of instability in such a flow was first analyzed by Yih [15,16] for flow down a rigid inclined plane using linear stability analysis. In particular, it was shown that the free-surface flow down a vertical rigid plate is always unstable at any nonzero Reynolds number, while for plates inclined at an angle, there is a nonzero critical Re beyond which the flow is unstable in the long-wave limit.

In the case of two-layer flow down an inclined plane, the interaction between the two interfaces renders the flow unstable [1,2,6,7] even at zero Reynolds number. When the rigid substrate over which the liquid layer is flowing is lined with a soft deformable solid layer, the coupling of deformation occurring in the soft wall with the dynamical variables governing the fluid flow could potentially lead to

*Author to whom all correspondence should be addressed: vshankar@iitk.ac.in

the stabilization of the free surface [13]. However, since an additional interface (i.e., liquid-solid) has been introduced that itself is deformable, there could be potential destabilization of the liquid-solid interface [17] as well. In the creeping-flow limit, the coupling arises solely due to the continuity conditions imposed at the fluid-solid interface. Thus, while the deformable solid layers are considered in the interest of suppressing the free-surface and interfacial instabilities, the liquid-solid interface itself can get destabilized in this process. In particular, Shankar and Sahu [13] carried out a linear stability analysis on a Newtonian liquid flowing down an inclined plane lined with a deformable solid layer, modeled as linear viscoelastic solid [18], and they showed that the deformability of the solid layer always has a stabilizing effect on the free-surface instability in the long-wave limit. However, at finite wave numbers, an increase in the nondimensional parameter Γ (which represents the elasticity of the solid layer) above its critical value leads to the destabilization of either the free-surface instability or the liquid-solid interface. However, Shankar and co-workers [12,13] have shown that there exists a sufficient window of tuning parameters (mainly, the critical strain rate in a solid layer, or equivalently the shear modulus of the solid layer) wherein the free-surface instability is suppressed without destabilizing the liquid-solid interface.

Gkanis and Kumar [19,20] observed that while considering finite deformations in the deformable solid, necessary modifications must be made to the linear elastic model in order for a constitutive relation to be consistent with the principle of material-frame indifference [21,22]. They considered the neo-Hookean model instead of the linear viscoelastic model for a solid layer, which is a rigorous generalization of the Hookean elastic solid subjected to finite deformations. Gkanis and Kumar [23] have also analyzed the configuration used in Ref. [13] using the neo-Hookean model to describe the solid deformation. The creeping-flow limit was considered in which free-surface disturbances were found to destabilize the flow. The work of Gaurav and Shankar [24] extended the work Gkanis and Kumar [23] to a finite Reynolds number. At a finite Reynolds number, it was shown that for both of the solid models (linear viscoelastic and neo-Hookean), the free-surface instability in flow down a rigid plane can be suppressed at all wavelengths by the deformability of the solid layer, and that there exists a significant window in the shear modulus of the solid considered, for moderate values of solid thickness, where both modes remain stable for all wave numbers. Jain and Shankar [14] extended previous studies for the case of a viscoelastic liquid down an inclined plane lined with a deformable solid modeled as a linear viscoelastic solid. In contrast to Newtonian liquid, viscoelastic liquid flow becomes unstable even in the absence of inertia due to elastic effects in the fluid. The solid deformability is again found to have a stabilizing effect on the free-surface instability, and it can suppress this instability at all wave numbers when the solid becomes sufficiently deformable. The passive mode of manipulation by the deformable solid layer makes it feasible to be exploited in practical applications.

Gkanis and Kumar [25] carried out a linear stability analysis to examine the role of a depth-dependent modulus on the stability of the creeping flow of a Newtonian fluid past a linear elastic solid. Two different variations of the modulus

were considered: one in which the modulus of the solid is a continuous function of position, and the second in which there is flow past two adjacent solid layers. For the case of continuous variation of the modulus, they found that if the average modulus is the same, then the case when the higher modulus is close to the interface is more stable. The subsequent experimental work of Neelmegam *et al.* [26] on plane Couette flow also considered a solid bilayer, and it showed that the solid layer adjacent to the liquid layer has a dominant effect on the liquid-solid interfacial instability, in broad agreement with the predictions of Gkanis and Kumar [25]. In the present work, we explore the possibility of using a solid-bilayer as a possible candidate for manipulating the free-surface instability.

In what follows, we carry out a linear stability analysis for a liquid layer flowing down an inclined plane [15], where the rigid surface of the inclined plane is lined now with the deformable solid bilayer with each solid layer modeled as a linear viscoelastic solid. While the neo-Hookean model of a solid is known to take into account the nonlinearities originating for finite deformation in a solid layer, in the present analysis we will restrict ourselves to the linear viscoelastic model of a solid so as to obtain the qualitative behavior of free-surface and liquid-solid interfacial instability with respect to the deformation in the solid layer. We also thereby extend the earlier study of [13] to the case of a solid bilayer, and we demonstrate that the bilayer offers significantly more control on the free-surface instability. A long-wave analysis is used to demonstrate the stabilizing role of the solid bilayer, and the long-wave results are continued to finite wavelengths using a numerical solution of the coupled governing stability equations.

The rest of this paper is divided into four sections: Section II describes the equations governing the three-layer system and the associated boundary conditions. The base state solutions and the coupled linearized governing equations and boundary conditions are also discussed in this section in brief. Section III presents the discussion on the asymptotic results obtained from solving the governing equations in the low-wave-number regime. Appendix A provides the details of the asymptotic analysis, and it demonstrates how the wave speed is determined using asymptotic analysis. Section IV is divided into two subsections: Sec. IV A deals with the description of the numerical procedure used for solving the obtained fourth-order ordinary differential equations, while Sec. IV B provides a detailed discussion of the results obtained. Finally, we end the paper by summarizing the key conclusions in Sec. V. Appendixes A and B provide additional details on the asymptotic analysis and the numerical procedure employed in this study.

II. PROBLEM FORMULATION

A. Governing equations

The three-layer system is comprised of a deformable solid bilayer with both of the constituent layers modeled as linear viscoelastic solids in the present study (Fig. 1) and a layer of Newtonian liquid flowing over the bilayer. The lower solid is assumed to be perfectly bonded to a rigid surface at $z^* = (1 + H)R$, which is inclined at an angle θ . In the unperturbed state,

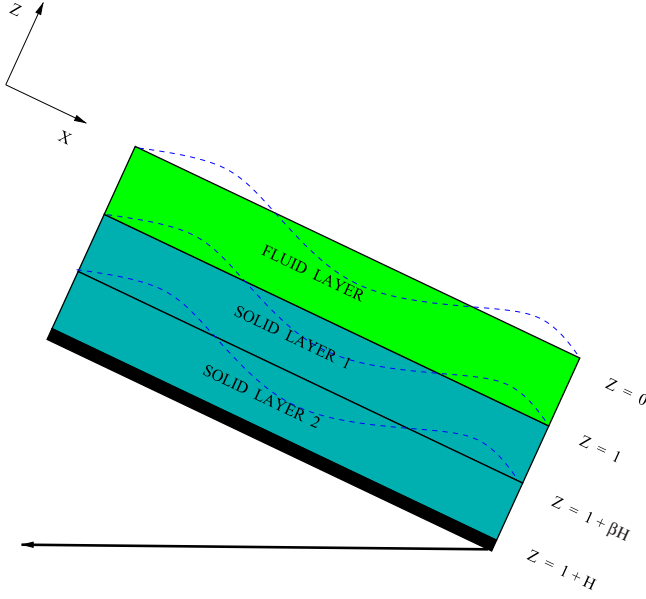


FIG. 1. Schematic diagram explaining the system under consideration and the nondimensional coordinate system used.

the lower solid layer occupies the region $(1 + \beta H)R < z^* < (1 + H)R$, and the upper solid layer is present in the region $1 < z^* < (1 + \beta H)R$. The liquid layer flows over the upper solid layer under the influence of gravity, and it is exposed to a passive gas at the unperturbed free surface $z^* = 0$. Here, a superscript asterisk has been used to denote all the dimensional variables.

Considering unidirectional and steady flow in the base state, with the solid layers at rest, the liquid film flows in the x direction with the velocity distribution

$$\bar{v}_x(z^*) = \frac{\rho g \sin \theta}{2\eta} (R^2 - z^{*2}). \quad (1)$$

The parameters used are defined as follows: ρ is the density of the liquid, η is its viscosity, g is the acceleration due to gravity, and θ is the inclination angle. The average velocity of the flow in the liquid layer can be given by $\bar{V}_a = \rho g R^2 \sin \theta / 3\eta$. The following scales are used to nondimensionalize various dynamical quantities: the thickness of the fluid R is used for lengths and displacements, the average velocity of the laminar flow \bar{V}_a is used for velocities, R/\bar{V}_a for time, and $\eta \bar{V}_a / R$ for stresses and pressure.

The liquid is assumed to be incompressible and Newtonian, hence the nondimensional equations governing the liquid flow are, respectively, the continuity equation and Navier-Stokes momentum equations:

$$\partial_x v_x + \partial_z v_z = 0, \quad (2)$$

$$\text{Re}[\partial_t + v_x \partial_x + v_z \partial_z]v_x = -\partial_x p + 3 + \nabla^2 v_x, \quad (3)$$

$$\text{Re}[\partial_t + v_x \partial_x + v_z \partial_z]v_z = -\partial_z p + 3 \cot \theta + \nabla^2 v_z, \quad (4)$$

where ∂_t is given by $\partial/\partial t$ and similar definitions hold for ∂_x and ∂_z , and $\nabla^2 = (\partial_x^2 + \partial_z^2)$. The variation of the physical quantities is neglected in the y direction, since we restrict ourselves to two-dimensional disturbances in the x - z plane in the present study. The Reynolds number used in Eqs. (3)

and (4) is defined as $\text{Re} = \rho \bar{V}_a R / \eta$. Since the flow is gravity-driven, the contribution due to the gravitational body force enters through the terms 3 and $3 \cot \theta$ appearing in the x and z momentum equations, respectively. The total stress tensor in the liquid layer can be written as $T_{ij} = -p \delta_{ij} + \tau_{ij}$, where p is the isotropic pressure, and $\tau_{ij} = (\partial_i v_j + \partial_j v_i)$ is the deviatoric stress tensor for the Newtonian liquid. The liquid-gas interface is exposed to a passive gas and can be treated as a free surface, as the shear stress exerted by the gas is negligible. When the interface is perturbed about its base state location $z = 0$, the dynamics of the position of the interface [$z = h(x)$] follows the well-known kinematic condition

$$\partial_t h + v_x \partial_x h = v_z. \quad (5)$$

The deformation in the solid bilayer is considered to be small, and therefore the linear viscoelastic solid model is used to describe the deformation dynamics in the solid. Although the neo-Hookean solid model is more accurate [19], many of the qualitative conclusions of the present study are expected to hold even for the more accurate neo-Hookean model. The dynamics of the solid layer can be represented by a displacement field u_i , which physically represents the deviation of the material points from their base-state positions. The velocity field in the solid layer is given by $v_i = \partial_t u_i$. In the interest of brevity, we provide the governing equations for both solids below, without indicating the dynamical variables with different subscripts for the two solid layers. When we carry out the linear stability analysis, the displacement fields in the two solid layers will be distinguished by a subscript. Both of the solid layers are assumed to be incompressible, and the respective displacement field satisfies

$$\partial_i u_i = 0. \quad (6)$$

The nondimensional Cauchy momentum equation in the two solid layers is given by

$$\text{Re} \partial_t^2 u_i = \partial_j \Pi_{ij} + 3 \frac{\hat{g}_i}{\sin \beta}. \quad (7)$$

Analogous to the liquid layer, the total stress tensor in the solid layer, Π_{ij} , is given by a sum of isotropic pressure p_g and a deviatoric stress σ_{ij} , $\Pi_{ij} = -p_g \delta_{ij} + \sigma_{ij}$, where \hat{g}_i is the unit vector pointing in the direction of gravity. The deviatoric stress σ_{ij} can be further represented by a sum of elastic and viscous stresses in the solid layers as $\sigma_{ij} = (1/\Gamma + \eta_r \partial_t)(\partial_i u_j + \partial_j u_i)$. Here, the nondimensional parameter Γ represents the (inverse) elasticity of the solid layers, $\Gamma = \bar{V}_a \eta / (GR)$, and $\eta_r = \eta_w / \eta$ is the ratio of solid to fluid viscosities. Note that the shear modulus G and viscosity η_w correspond to the solid layer under consideration. From this point onward, subscript 1 is used to denote the variables corresponding to the top solid layer, and subscript 2 is used to denote the variables corresponding to the bottom solid layer. For simplicity, we set the densities of both solid layers to be the same as the density of the liquid layer. Many soft elastomers have densities that are very close to the density of liquids such as water. Further, as we demonstrate below, the instability (and its suppression) is primarily brought out by an asymptotic analysis in the low-wave-number limit. In this limit, the inertial stresses in the solid layers are proportional to k^2 , and hence they are negligible. Even if the densities of the two solids are

different, the density contrast will be subdominant in the low- k regime. There will be some effect of the density contrast when $k \sim O(1)$, but the qualitative predictions obtained for equal densities are expected to be valid even for the case when there is a density contrast.

The boundary conditions to be used are given as follows: The lower solid layer is assumed to be perfectly bonded to the rigid surface at $z = (1 + H)$, and so zero displacement conditions apply at this surface. The conditions at the perturbed liquid-solid interface are the continuity of velocities and stresses at this interface. The boundary conditions at the solid-solid interface at $z = 1 + \beta H$ are the continuity of the displacement fields and stress balance in the two solid layers.

B. Base state

The steady velocity and the pressure field in the liquid layer under laminar conditions are given by

$$\bar{v}_x = \frac{3}{2}(1 - z^2), \quad (8)$$

$$\bar{p} = 3z \cot \theta. \quad (9)$$

These base flow quantities here and henceforth will be represented by an overbar. The shear stresses at the liquid-solid interface $z = 1$ along with gravitational body force drives the deformation in the solid, and the corresponding displacement field is given by

$$\bar{u}_{x1} = \frac{3\Gamma_1}{2}[(1 + \beta H)^2 - z^2], \quad (10)$$

where $\Gamma_1 \equiv \bar{V}_a \eta / (G_1 R)$. The pressure field results only from the gravitational body force and therefore can be represented by

$$\bar{p}_{g1} = 3z \cot \theta. \quad (11)$$

Similarly, the base state variables in the lower solid layer are given by

$$\bar{u}_{x2} = \frac{3\Gamma_2}{2}[(1 + H)^2 - z^2], \quad (12)$$

$$\bar{p}_{g2} = 3z \cot \theta, \quad (13)$$

where $\Gamma_2 \equiv \bar{V}_a \eta / (G_2 R)$.

C. Linear stability analysis

A temporal linear stability analysis is used to analyze the stability of the present problem. Small perturbations (denoted by primed quantities) are imposed on a given dynamical quantity as $\phi = \bar{\phi} + \phi'$, and the perturbed quantity ϕ' is expanded in the form of Fourier modes in the x direction having an exponential dependence in time:

$$\phi'(x, z, t) = \tilde{\phi}(z) \exp[ik(x - ct)]. \quad (14)$$

The governing parameters used are defined as follows: k is the wave number of the perturbations, c is a complex wave speed that represents the growth of perturbations, and $\tilde{\phi}(z)$ is the eigenfunction of the dynamical variable in consideration and can be determined while solving the framed linearized differential equations using linear stability analysis. As mentioned earlier, only two-dimensional perturbations are considered here. The complex wave speed $c = c_r + ic_i$, where the real

part c_r represents the phase velocity of perturbations, and the imaginary part c_i governs the growth or decay of perturbations. The given base state is considered to be temporally unstable when $c_i > 0$.

The linearization of the governing equations (2)–(7), around the base state (8), is obtained by substituting the above expansion (14). We define the operator $\mathcal{L} \equiv (d_z^2 - k^2)$, which recurs in the following set of equations. The linearized equations obtained for the liquid layer are

$$d_z \tilde{v}_z + ik \tilde{v}_x = 0, \quad (15)$$

$$\text{Re}[ik(\bar{v}_x - c)\tilde{v}_x + (d_z \bar{v}_x)\tilde{v}_z] = -ik\tilde{p} + \mathcal{L}\tilde{v}_x, \quad (16)$$

$$\text{Re}[ik(\bar{v}_x - c)\tilde{v}_z] = -d_z \tilde{p} + \mathcal{L}\tilde{v}_z. \quad (17)$$

The above equations are combined to give a fourth-order ordinary differential equation, which is essentially the Orr-Sommerfeld equation for the dynamical variable \tilde{v}_z :

$$ik \text{Re}[(\bar{v}_x - c)\mathcal{L} - d_z^2 \bar{v}_x]\tilde{v}_z = \mathcal{L}^2 \tilde{v}_z. \quad (18)$$

The linearized stability equations for the displacement field in the upper solid layer are

$$d_z \tilde{u}_{z1} + ik \tilde{u}_{x1} = 0, \quad (19)$$

$$-\text{Re} k^2 c^2 \tilde{u}_{x1} = -ik \tilde{p}_{g1} + \left(\frac{1}{\Gamma_1} - ikc\eta_{r1}\right) \mathcal{L}\tilde{u}_{x1}, \quad (20)$$

$$-\text{Re} k^2 c^2 \tilde{u}_{z1} = -d_z \tilde{p}_{g1} + \left(\frac{1}{\Gamma_1} - ikc\eta_{r1}\right) \mathcal{L}\tilde{u}_{z1}, \quad (21)$$

and the fourth-order differential equation for \tilde{u}_{z1} is given by

$$(1 - ikc\eta_{r1}\Gamma_1)\mathcal{L}^2 \tilde{u}_{z1} + \text{Re} k^2 c^2 \Gamma_1 \mathcal{L}\tilde{u}_{z1} = 0. \quad (22)$$

In a similar manner, the linearized equations for the lower solid layer are given by

$$d_z \tilde{u}_{z2} + ik \tilde{u}_{x2} = 0, \quad (23)$$

$$-\text{Re} k^2 c^2 \tilde{u}_{x2} = -ik \tilde{p}_{g2} + \left(\frac{1}{\Gamma_2} - ikc\eta_{r2}\right) \mathcal{L}\tilde{u}_{x2}, \quad (24)$$

$$-\text{Re} k^2 c^2 \tilde{u}_{z2} = -d_z \tilde{p}_{g2} + \left(\frac{1}{\Gamma_2} - ikc\eta_{r2}\right) \mathcal{L}\tilde{u}_{z2}, \quad (25)$$

and the corresponding fourth-order differential equation for \tilde{u}_{z2} is given by

$$(1 - ikc\eta_{r2}\Gamma_2)\mathcal{L}^2 \tilde{u}_{z2} + \text{Re} k^2 c^2 \Gamma_2 \mathcal{L}\tilde{u}_{z2} = 0. \quad (26)$$

The kinematic equation (5) can be expressed in terms of the Fourier modes as

$$ik(\bar{v}_x|_{z=0} - c)\tilde{h} = \tilde{v}_z|_{z=0} \quad (27)$$

by substituting $h(x, t) = \tilde{h} \exp[ik(x - ct)]$ and linearizing the other dynamical quantities at $z = 0$. The evolution of the interface position is now described by the Fourier expansion coefficient \tilde{h} . The linearized tangential stress and normal stress condition at $z = 0$ are obtained by Taylor-expanding the boundary conditions at the perturbed free-surface interface about $z = 0$ to give

$$-3\tilde{h} + (d_z \tilde{v}_x + ik \tilde{v}_z) = 0, \quad (28)$$

$$-\tilde{p} - 3\tilde{h} \cot \beta + 2d_z \tilde{v}_z - k^2 \Sigma \tilde{h} = 0. \quad (29)$$

The nondimensional parameter Σ used is defined as $\Sigma = \gamma/(\bar{V}_a\eta)$ and represents the nondimensional surface tension between the liquid and the gas, considering γ as the dimensional surface tension. It could easily be deduced that while linearizing, an additional contribution arises in the boundary conditions that is proportional to $-3\bar{h}$ and couples the base laminar flow with the height fluctuations of the free interface.

The velocity and stress continuity conditions are linearized about the interface $z = 1$ to obtain

$$\tilde{v}_z = -ikc\tilde{u}_{z1}, \quad (30)$$

$$\tilde{v}_x + d_z\tilde{v}_x|_{z=1}\tilde{u}_{z1} = -ikc\tilde{u}_{x1}, \quad (31)$$

$$d_z\tilde{v}_x + ik\tilde{v}_z = \left(\frac{1}{\Gamma_1} - ikc\eta_{r1}\right)[d_z\tilde{u}_{x1} + ik\tilde{u}_{z1}], \quad (32)$$

$$\begin{aligned} -\tilde{p} + 2d_z\tilde{v}_z &= -\tilde{p}_{g1} + 2\left(\frac{1}{\Gamma_1} - ikc\eta_{r1}\right)d_z\tilde{u}_{z1} \\ &\quad -k^2\Sigma_1\tilde{u}_{z1}, \end{aligned} \quad (33)$$

where Σ_1 is the nondimensional interfacial tension between the liquid and upper solid layers. It can be verified that the interface position can be represented as $\tilde{g} = \tilde{u}_{z1}|_{z=1}$ within the realm of the linear stability analysis. The interaction of the first derivative of base velocity with the displacement field in the upper solid layer, appearing in Eq. (31), results from the Taylor expansion of the velocity about the unperturbed interface $z = 1$. Kumaran [17] showed that this interaction is responsible for destabilizing the fluid-solid interface.

The conditions at the interface between the two solid layers are given by the continuity of displacements and stresses at $z = (1 + \beta H)$:

$$\tilde{u}_{z1} = \tilde{u}_{z2}, \quad (34)$$

$$\tilde{u}_{x1} = \tilde{u}_{x2}, \quad (35)$$

$$\begin{aligned} \left(\frac{1}{\Gamma_1} - ikc\eta_{r1}\right)[d_z\tilde{u}_{x1} + ik\tilde{u}_{z1}] &= \left(\frac{1}{\Gamma_2} - ikc\eta_{r2}\right)[d_z\tilde{u}_{x2} \\ &\quad + ik\tilde{u}_{z2}], \end{aligned} \quad (36)$$

$$\begin{aligned} -\tilde{p}_{g1} + 2\left(\frac{1}{\Gamma_1} - ikc\eta_{r1}\right)d_z\tilde{u}_{z1} &= -\tilde{p}_{g2} \\ &\quad + 2\left(\frac{1}{\Gamma_2} - ikc\eta_{r2}\right)d_z\tilde{u}_{z2} \end{aligned} \quad (37)$$

$$-k^2\Sigma_2\tilde{u}_{z2}, \quad (38)$$

where Σ_2 is the nondimensional surface tension between the two solid layers.

The lower solid layer is bonded to the rigid inclined plane, and thus the corresponding displacement field follows the no-slip boundary conditions at $z = (1 + H)$ and is given by

$$\tilde{u}_{z2} = 0, \quad \tilde{u}_{x2} = 0. \quad (39)$$

The stability of the three-layer configuration under consideration has now been fully specified with these linearized governing equations and boundary conditions. The complex wave speed c is an unknown eigenvalue that is a function of Re , k , Γ_{eff} , β , H , surface tensions, and viscosity ratios. The linearized equations are solved numerically in general, for

arbitrary values of k and Re . A long-wave asymptotic analysis is considered first for the present problem, similar to the classic analysis of Yih [15], to obtain analytically tractable solutions in this limit.

III. LOW-WAVE-NUMBER ASYMPTOTIC ANALYSIS

The results of the low-wave-number asymptotic analysis, carried out along the lines of the analysis used by Yih [15], are presented in this section. The goal of this asymptotic analysis is to understand the effect of wall layer deformability on the disturbances of the liquid-gas interface. The wavelength of the disturbances is considered to be large in the asymptotic analysis when compared to the widths of the various layers present, and therefore the condition $k \ll 1/(1 + H)$ should be met in order for the analysis to be valid. This relation reduces to $k \ll 1$ [in the case of $H \sim O(1)$] and $k \ll 1/H$ (in the case of $H \gg 1$) for two extreme values of H chosen. Thus, for larger values of H , the long-wave analysis is valid at much smaller values of k . The total solid-layer thickness H is considered to be an $O(1)$ quantity in the present analysis, and therefore the low-wave-number limit $k \ll 1$ is considered here. For $k \ll 1$, the complex wave speed can be expanded in an asymptotic series in k as

$$c = c^{(0)} + kc^{(1)} + \dots \quad (40)$$

In this study, the leading-order wavespeed and the $O(k)$ correction to c are sufficient to determine the stability of the disturbances in the low-wave-number regime. This asymptotic analysis closely resembles the one previously carried out by Shankar and Sahu [13]. Here, we present the main results obtained from the asymptotic analysis, and the details are presented in Appendix A. The leading-order and first corrections to the wave speed obtained are

$$c^{(0)} = 3, \quad (41)$$

$$c^{(1)} = i\left(\left[\frac{6}{5}\text{Re} - \cot\beta\right] - 9[\Gamma_1\beta + \Gamma_2(1 - \beta)]H\right). \quad (42)$$

The stability of the system is governed by the evolution of disturbances, and $c^{(1)}$, being a purely imaginary quantity, dictates this evolution. The validity of the asymptotic solution could be checked with the terms involving Re and $\cot\beta$, which were reported by Yih [15] as well as Shankar and Sahu [13]. These terms correspond to the free-surface instability in the liquid layer flowing down a rigid inclined plane for the case when $\frac{6}{5}\text{Re} > \cot\beta$.

The effect of the solid-layer deformability on the free-surface instability mode comes into effect with the involvement of Γ_1 and Γ_2 . It is useful to reinterpret this result using the ‘‘effective modulus’’ of the solid bilayer defined as $H/G_{\text{eff}} = H_1/G_1 + H_2/G_2$, and further define $\Gamma_{\text{eff}} = \bar{V}\eta/(G_{\text{eff}}R)$ based on this effective shear modulus. This implies that $[\Gamma_1\beta + \Gamma_2(1 - \beta)]H$ in Eq. (42) can be replaced with $\Gamma_{\text{eff}}H$. This term occurs with a negative sign implying that the solid bilayer always has a stabilizing effect on the free-surface instability.

In the limit of a rigid solid layer, the effective shear modulus $G_{\text{eff}} \rightarrow \infty$, and therefore Γ_{eff} approaches zero. From a mathematical viewpoint, it can be easily understood that the contribution from the deformable solid bilayer vanishes when either $\Gamma_{\text{eff}} \rightarrow 0$ or $H = 0$. However, both cases relate to the

absence of the deformable layer and therefore would not be considered further in this study. Under the criterion

$$9\Gamma_{\text{eff}}H > \left(\frac{6}{5}\text{Re} - \cot\beta\right), \quad (43)$$

the free-surface instability is completely stabilized in the long-wave limit. This result bears a striking resemblance to the earlier asymptotic result [13] for a single layer, with Γ_{eff} replacing Γ in the earlier work. This relation also serves as a consistency check to our numerical solutions in the long-wave limit. Further, the dissipative stresses in the solid layers are subdominant in the low- k limit compared to elastic stresses in the solid layers, and hence they will not affect the result for c_i in this limit. However, at finite wave numbers, as we show in the next section, the dissipative stresses in the solid layers also play a critical role in determining the stability of the system.

Interestingly, the above asymptotic result shows that the stabilization of the free-surface instability is influenced only by the effective modulus G_{eff} , and hence it is unaffected by the relative placement of the two solid layers with respect to the liquid layer. In other words, the stabilizing nature of the bilayer would be present even if the two solid layers were to be flipped. This is one of the main results of the present study. It is pertinent to discuss whether this prediction for a bilayer solid would be valid even for the case of a single solid layer with a continuously varying modulus [25]. While a precise answer to this question would require a similar analysis of that configuration, it is nonetheless possible to speculate that the stabilizing nature of the solid would be independent of the direction of variation of modulus in cases in which the modulus is continuously varying, when the average modulus is kept the same.

However, the predictions of the asymptotic analysis are valid only in the limit of $k \ll 1$. In the following section, the prediction of the analysis is extended to arbitrary values of wave number k by a numerical solution.

IV. NUMERICAL SOLUTION

A. Solution methodology

A brief description of the numerical technique used to solve the governing equations and boundary conditions is presented here. The overall idea is to express the coupled fourth-order ordinary differential equations and the corresponding boundary conditions in terms of a matrix eigenvalue problem, with the complex wave speed c being the eigenvalue. The eigenvalue has been obtained by evaluating the roots of the characteristic equation, which in turn is obtained by setting the determinant of the matrix to zero. The convergence of the eigenvalue was achieved iteratively using the above procedure with the help of a Newton-Raphson iterative procedure. We start our numerical solution by taking the initial guess for the eigenvalue from asymptotic analysis, which is only valid in the low- k regime. The eigenvalue obtained from the above numerical computation acts as an initial guess for the next increment in wave number, and similarly this procedure is repeated for finite wave numbers. A more detailed description of the numerical technique is provided in Appendix B.

B. Results and discussion

As shown by the low- k analysis, the stabilization of the free-surface instability is achieved when Γ_{eff} is increased beyond a critical value. For higher values of Γ_{eff} when the solid layer is sufficiently deformable, the liquid-solid interface itself can potentially become unstable. This liquid-solid interfacial instability was reported in [13] for the case of free-surface flow down a single deformable layer. Moreover, a recent study on the stability of plane Couette flow past an elastic bilayer [26] showed that the instability of the liquid-solid interface is sensitive to the relative placement of the two solid layers. In particular, when the softer solid layer is adjacent to the liquid, the system is found to be more unstable. Interestingly, the low- k asymptotic results of the present study show that the *suppression* of the free-surface instability is determined only by the *effective* modulus of the solid layer, and it is independent of the relative placement of the two layers. Thus the two interfacial modes, i.e., the gas-liquid interfacial and liquid-solid interfacial modes, behave differently with respect to the relative placement of the two solid layers in the bilayer in the low-wave-number limit. This motivates us to explore the possibility of suppression of the free-surface instability without inducing additional instabilities at the liquid-solid interface by manipulating the relative placement and properties (i.e., shear modulus, viscosity, and thickness) of the two solid layers comprising the bilayer. This is addressed using the numerical solution of the linear stability equations. To capture the free-surface mode in the numerical solution, we use the low- k asymptotic results from the preceding section as a starting guess, and we use the numerical procedure outlined above to continue the low- k results to finite values of k . For the liquid-solid interfacial instability, which happens at finite k , we use a $\text{Re} = 0$ analysis (similar to [17], where an analytical solution is possible for arbitrary k) to identify the presence of the unstable liquid-solid interfacial mode. The solutions of the $\text{Re} = 0$ analysis reveal that the disturbances are stable in the creeping-flow limit for the present system, but when these solutions are further continued using numerical computations to nonzero values of Re , the liquid-solid interface becomes unstable at finite Re , which clearly shows that the instability induced at the liquid-solid interface occurs only because of inertia of the coupled solid-fluid system. Henceforth, this unstable mode is referred to as *inertial LS mode*. By way of nomenclature, we refer to the gas-liquid interfacial mode as the “GL” mode, and inertial liquid-solid interfacial disturbances as the “LS” mode in the ensuing discussion.

We next present numerical results in the c_i - k plane in order to demonstrate the origin and evolution of instabilities with wave number as the bilayer solid is made more deformable. This will assist us in understanding the evolution of both the GL and LS mode instabilities clearly as Γ_{eff} is increased. We define the ratio $G_r = G_2/G_1$, the ratio of bottom- to top-layer shear moduli of the two solids. Figure 2 shows the variation of the imaginary part of the wave speed c_i for the GL mode as a function of the wave number k , obtained from the asymptotic analysis and the numerical solution for fixed values of other parameters. The asymptotic result is correct only to $O(k)$, and it is expected to break down at $k \sim O(1)$. Our numerical solution agrees well with the asymptotic result in the low- k regime,

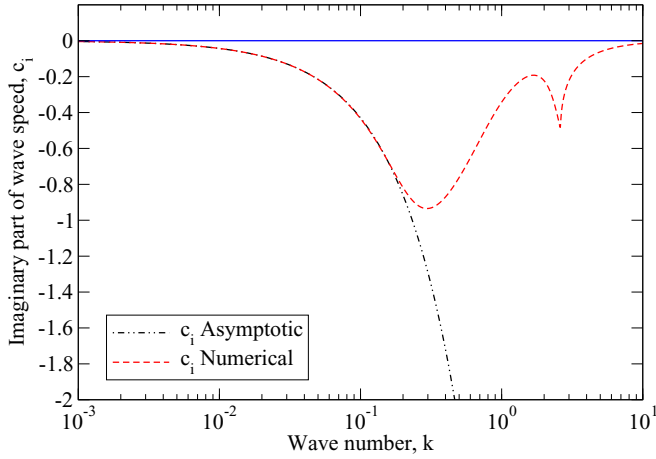


FIG. 2. Comparison of low- k asymptotic and numerical results for the GL mode: c_i vs k for $G_r = 1$, $\theta = \pi/4$, $\text{Re} = 1.0$, $H = 0.5$, $\beta = 0.5$, $\Gamma_{\text{eff}} = 1$, $\eta_{r1} = 0$, $\eta_{r2} = 0$, $\Sigma = 0$, $\Sigma_1 = 0$, and $\Sigma_2 = 0$. The horizontal line with $c_i = 0$ serves as a visual aid to demarcate stable and unstable regions.

but quickly starts to deviate from the asymptotic result for $k \sim 0.3$.

In Fig. 3, we show how c_i varies as a function of wave number for the GL mode as Γ_{eff} is increased for a given bilayer configuration with $G_r = 16$ (softer layer on top), and with both layers of equal thickness ($\beta = 0.5$). As predicted by the asymptotic analysis, as Γ_{eff} is increased, the free-surface mode is stabilized (i.e., $c_i < 0$) at low values of k . Also noteworthy is the fact that the free-surface mode is stabilized at all wave numbers when Γ_{eff} is increased up to 1. It is also interesting to observe that the c_i - k curves for $\Gamma_{\text{eff}} = 0, 0.5$, and 1 all merge at sufficiently higher values of $k \sim 10$, since at such small wavelengths the disturbances at the free surface decay rather rapidly, and hence the extent of deformability of the solid bilayer does not affect the decay rates of these small-wavelength fluctuations. An interesting feature emerges as Γ_{eff} is increased to 2.5, wherein we note first that the free-surface mode be-

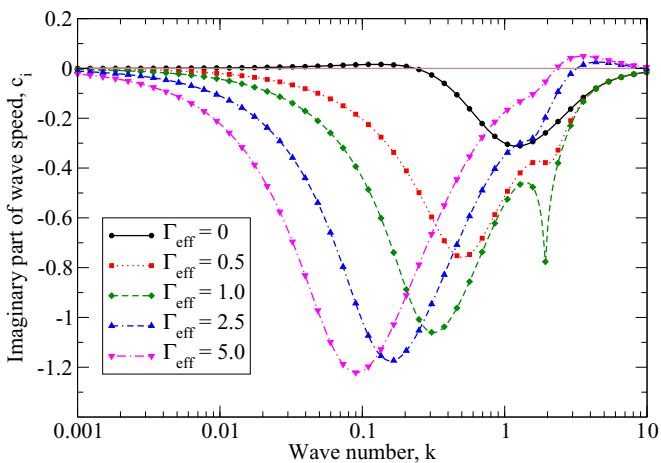


FIG. 3. c_i vs k for the GL mode for different values of Γ_{eff} : Data for $G_r = 16$, $\theta = \pi/4$, $\text{Re} = 1.0$, $H = 0.5$, and $\beta = 0.5$. The remaining parameters, viz., η_{r1} , η_{r2} , Σ , Σ_1 , and Σ_2 , are set to zero.

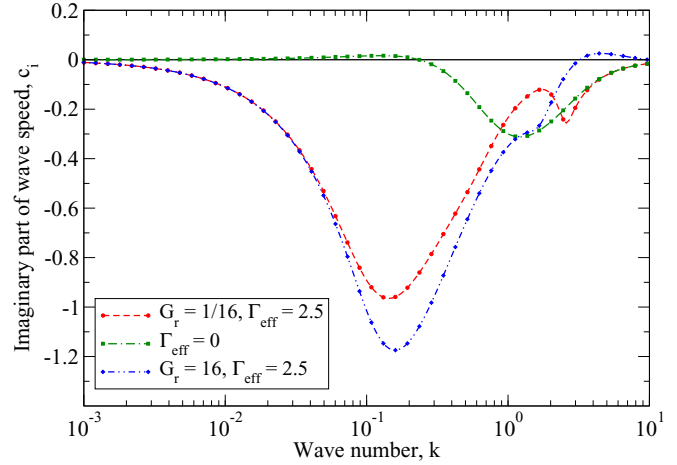


FIG. 4. c_i vs k for the GL mode for $\Gamma_{\text{eff}} = 2.5$: Data for $G_r = 16$ and $1/16$, $\theta = \pi/4$, $\text{Re} = 1.0$, $H = 0.5$, and $\beta = 0.5$. The remaining parameters, viz., η_{r1} , η_{r2} , Σ , Σ_1 , and Σ_2 , are set to zero.

comes unstable at finite values of $k \sim 2$, indicating that further decrease in the effective modulus of the bilayer leads to an instability at finite wave numbers, which is absent in flow down a rigid incline. Furthermore, as $k \sim 10$, for $\Gamma_{\text{eff}} = 2.5$ and 5, the c_i - k curves do not merge with the results obtained for $\Gamma_{\text{eff}} = 0, 0.5$, and 1. One might have expected that for such short-wave fluctuations, the c_i values at higher k must be independent of the extent of deformability Γ_{eff} . This suggests that at $k \gg 1$, the GL mode has transformed into a different mode. This change in behavior is attributed to a mode exchange phenomenon, which we discuss in detail later in relation to Fig. 6.

In Fig. 4, we analyze the role of solid deformability on the GL mode instability for a given configuration of the solid bilayer, as well as for the corresponding “flipped” configuration (where the softer and harder solid layers are interchanged). The other parameters are fixed as follows: $\theta = \pi/4$, $\text{Re} = 1.0$, $G_r = 16$ (softer layer adjacent to the

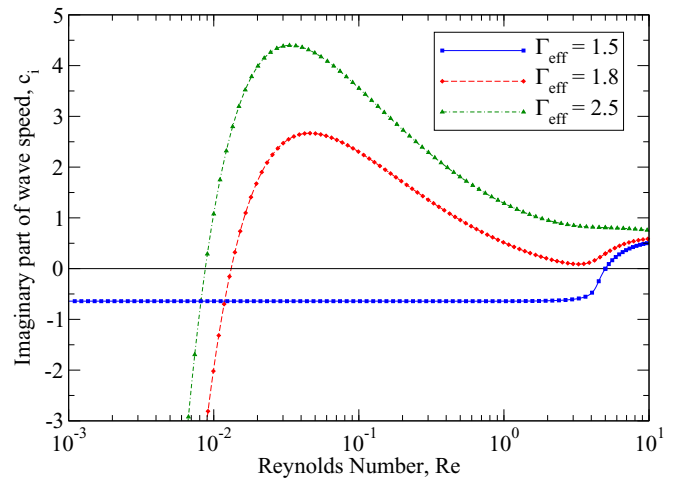


FIG. 5. Effect of solid-layer deformability on the inertial LS mode: c_i vs Re for $G_r = 1/50$, $\theta = \pi/4$, $\beta = 0.05$, $H = 0.5$, $k = 0.1$, and different values of Γ_{eff} . The remaining parameters, viz., η_{r1} , η_{r2} , Σ , Σ_1 , and Σ_2 , are set to zero.

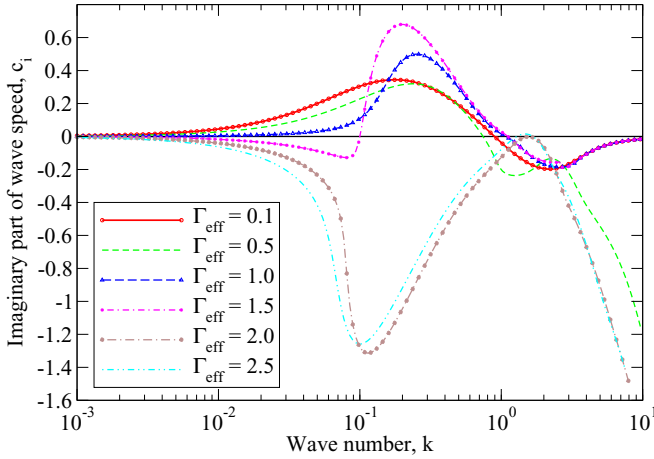


FIG. 6. Effect of solid-layer deformability on the two different interfacial modes present in the system at $\text{Re} = 5.0$: c_i vs k for $G_r = 1/50$, $\theta = \pi/4$, $\beta = 0.05$, $H = 0.5$, and different values of Γ_{eff} . The remaining parameters, viz., η_{r1} , η_{r2} , Σ , Σ_1 , and Σ_2 , are set to zero.

liquid layer), and for $G_r = 1/16$ (harder layer adjacent to the liquid layer). When $\Gamma_{\text{eff}} = 0$ (rigid inclined plane), c_i is positive (free surface is unstable) from $k \ll 1$ to $k \sim 0.3$, and for larger values of k the system is stable. We have set the nondimensional gas-liquid surface tension $\Sigma = 0$, since even the flow down a rigid inclined plane is stable for $k > 0.3$. A nonzero gas-liquid surface tension Σ would stabilize only higher wave-number perturbations. For $G_r = 1/16$, as Γ_{eff} is increased to 2.5, the instability is suppressed by the solid bilayer at all wave numbers. However, for the flipped configuration with $G_r = 16$, when Γ_{eff} is further increased to 2.5, we find that the perturbations with $k \sim 2.5$ are destabilized by the deformability of the solid layer. Thus, when the softer solid is adjacent to the fluid layer, at sufficiently higher values of Γ_{eff} , the GL mode is destabilized at finite k , while perturbations with similar wavelengths are stable in a rigid inclined plane, clearly indicating the destabilizing nature of the deformable solid layer. Interestingly, when the bilayer is flipped ($G_r = 1/16$), the free-surface mode is found to be stable at all wave numbers for the same value of Γ_{eff} , clearly suggesting that the finite- k behavior is very sensitive to the relative placements of the two solid layers in the bilayer.

We next turn our attention to the possibility of the existence of another unstable mode due to the instability of the liquid-solid interface. As mentioned earlier, we use a zero- Re analysis, wherein it is possible to obtain an analytical solution to the wavespeed in that limit. One of the solutions to c corresponds to the GL interfacial mode, and the other solution pertains to the liquid-solid (LS) interface. Our analysis shows that this mode is stable in the limit of zero Re , unlike the case of plane Couette flow [17], wherein the flow destabilizes the liquid-solid interfacial mode even at $\text{Re} = 0$. However, as we continue this mode to finite Re (Fig. 5), we find that the mode does get destabilized due to wall deformability. It is more accurate to characterize these modes as the “inertial LS” modes since the results clearly demonstrate that the instability exists only for nonzero values of Re , and inertial effects are required in the fluid and solid for destabilization.

Figure 6 shows the behavior of the GL mode at higher Re for different values of Γ_{eff} . As Γ_{eff} increases from 1.5 to 2.0, there is a qualitative change in the behavior of the variation of c_i with k . For Γ_{eff} up to 1.5, at sufficiently large $k \sim 10$, all the curves for different values of Γ_{eff} merge with each other. As mentioned above, this is to be expected since the c_i variation with k is shown for the GL mode, and for large k the interfacial disturbances would be confined locally to the gas-liquid interface, hence any change in the deformable nature of the solid should not have an effect on the GL modes at high k . Instead, for $\Gamma_{\text{eff}} > 1.5$, at higher values of k , the c_i variation with k (for $k \gg 1$) differs significantly, even when the $k \ll 1$ results for all the modes have the same behavior with $|c_i| \rightarrow 0$. The behavior seen in this figure is typical of “exchange” of the two modes present in the system (the GL mode and the inertial LS mode) at finite values of fluid inertia. Such exchanges between the two modes coexisting in the system have been observed in earlier studies as well; see, for example, Gaurav and Shankar [24].

Although such exchanges between the modes are often encountered in the context of hydrodynamic stability, the nature of the exchange is quite intriguing. To understand this in detail, we demonstrate the above phenomenon of mode exchange in Fig. 7, in which we focus on the sudden change in behavior of the respective modes. The mode exchange starts after $\Gamma_{\text{eff}} = 1.5$, and it could be clearly noted that at the point of exchange, near $k \sim 0.9$, the behavior of c_i versus k is smooth for $\Gamma_{\text{eff}} = 1.5$. As soon as Γ_{eff} is increased to 1.8, the c_i - k behavior shows a cusp, and upon further increase of Γ_{eff} , the mode exchange occurs. When Γ_{eff} is increased further, beyond 2.0, the GL and the inertial LS modes are found to be totally independent of each other while coexisting in the system. No exchange of modes was found after increasing Γ_{eff} beyond 2. This figure further suggests that labeling the two modes as GL and LS at finite values of Γ_{eff} is somewhat arbitrary, and it depends on whether one considers the behavior of the mode to be consistent with $k \ll 1$ or $k \gg 1$. Before the mode exchange,

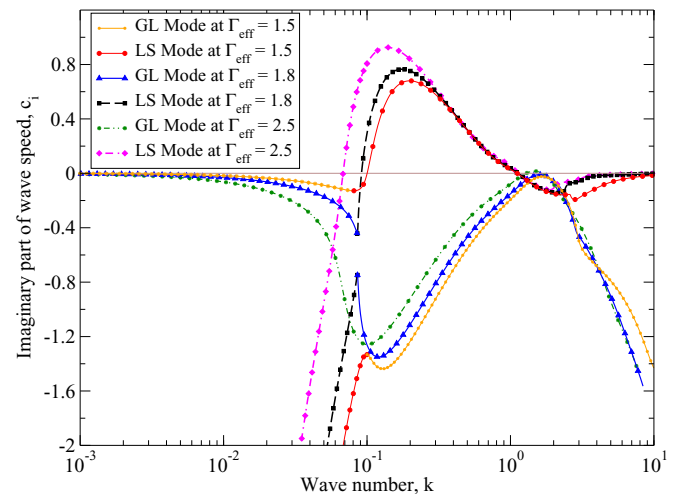


FIG. 7. Mode exchange phenomenon at $\text{Re} = 5.0$: c_i vs k for $G_r = 1/50$, $\theta = \pi/4$, $\beta = 0.05$, $H = 0.5$, and different values of Γ_{eff} . The remaining parameters, viz., η_{r1} , η_{r2} , Σ , Σ_1 , and Σ_2 , are set to zero.

the GL mode has a characteristic value as $k \rightarrow 0$, and the c_i values tend to each other for $k \gg 1$ for different values of Γ_{eff} . However, after mode exchange, if we use the high- k behavior to identify the GL mode, then because of mode exchange, this mode does not continue all way to $k \ll 1$ with the behavior expected for a GL mode. Instead, at some intermediate (but finite) k , this mode takes on the behavior of the LS mode. The same holds for the low- k limit as well: if we identify a mode based on its behavior at low values of k , when this is continued to higher values, it does not approach the value expected for a GL mode, but indeed approaches the high- k value appropriate for the LS mode.

This discussion goes on to show that at finite values of Re and Γ_{eff} , it is difficult to label a given mode as GL or LS, since the behavior gets interchanged. With this, we end our discussion on the two modes in the system, and we proceed to present the complete picture of the two modes in the $\Gamma_{\text{eff}}-k$ plane, clearly demarcating the boundaries between the stable and unstable regions. This would also provide us with an unambiguous method to identify the suitable range of the nondimensional parameter Γ_{eff} in order to induce or suppress the instabilities.

We first consider the case of equal thickness of the two solid layers. Figure 8 depicts the neutral stability curves (where the imaginary part of the wave speed $c_i = 0$) for two values of G_r (corresponding to two bilayer configurations that are flipped versions of each other). We examine the effect of solid-layer deformability on this configuration. Consider first the bottom left neutral stability curve and choose any k value in this region. As Γ_{eff} is increased beyond 0.065, there is a transition from unstable to stable perturbations of the GL mode. Similarly, if we consider the top right neutral stability curve, for a given wave number of 10, the GL mode will face a transition from stable to unstable disturbances at either 30 or 1.5 depending upon the G_r value used. There is a large region in Γ_{eff} (for fixed values of other parameters), which translates into a large region in the shear modulus of the effective combination of the solid layer, where the GL mode is stabilized by the solid-layer

deformability. Thus, a large “window” in the parameter space is available for the choice of Γ_{eff} for the system to be stable at all wave numbers.

Moreover, Fig. 8 focuses on the effect of solid-layer deformability on the GL mode (the bottommost curves and the two curves on the top) and the LS mode (the middle curves) -type instabilities present in the system. We observe that qualitatively it is only the effective shear modulus of both of the solid layers and not the individual shear moduli that affects the bottommost curves for the GL mode, as predicted by the low- k asymptotic analysis. However, the other curves are sensitive to the placement of the two layers with respect to the fluid. The results show that the instabilities can be delayed to a certain extent when we use a hard solid adjacent to a fluid layer ($G_r = 1/16$) compared to the case when it is not ($G_r = 16$). This also demonstrates that the presence of a hard solid layer adjacent to a fluid layer has a stabilizing effect on the GL interfacial instability.

Figure 9 deals with the flipping of the two solid layers when the thickness ratio of the two layers is not unity (i.e., $\beta \neq 0.5$, solid layers with unequal thickness). We have kept all the parameters to be the same, other than the ratio of the thickness of the two solid layers, β . Our objective is to analyze the effect of the relative thickness of two solid layers on the various instabilities. As the top-layer thickness is decreased, we found a destabilizing effect on the GL mode instabilities, though the LS mode instabilities remained unaffected. However, even for $\beta \neq 0.5$, the general trend seems to be that when the solid layer adjacent to the fluid is harder, the GL and LS upper neutral curves shift upward, indicating a stabilizing effect.

The low- k asymptotic analysis further indicated that the solid-fluid viscosity ratio η_r is sub-dominant in that limit, and hence does not affect the stabilization at low k . In Fig. 10, we examine the effect of changing η_{r1} (i.e., the ratio of the viscosity of the top solid layer to the viscosity of the fluid) on the neutral stability curves. When $G_r = 1/50$ (harder layer on top), an increase in η_{r1} (the viscosity ratio of the hard layer) has virtually no effect on the lower neutral curve,

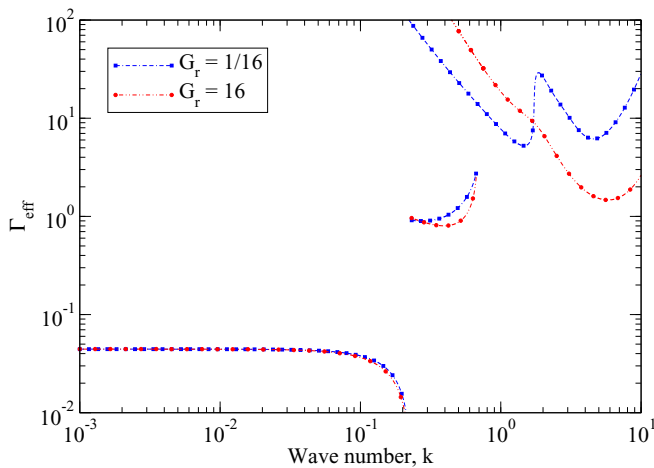


FIG. 8. Neutral stability curves for the GL and LS modes of instability in the $\Gamma_{\text{eff}}-k$ plane: $G_r = 1/16$ and 16, $\theta = \pi/4$, $\beta = 0.5$, $\text{Re} = 1.0$, and $H = 0.5$. The remaining parameters, viz., η_{r1} , η_{r2} , Σ , Σ_1 , and Σ_2 , are set to zero.

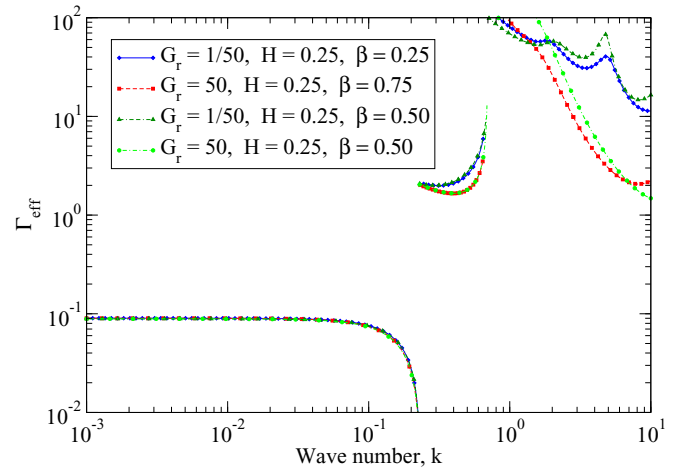


FIG. 9. Neutral stability curves for the GL and LS modes of instability in the $\Gamma_{\text{eff}}-k$ plane: $G_r = 1/50$ and 50, $\theta = \pi/4$, $\text{Re} = 1.0$, and $H = 0.25$. The remaining parameters, viz., η_{r1} , η_{r2} , Σ , Σ_1 , and Σ_2 , are set to zero.

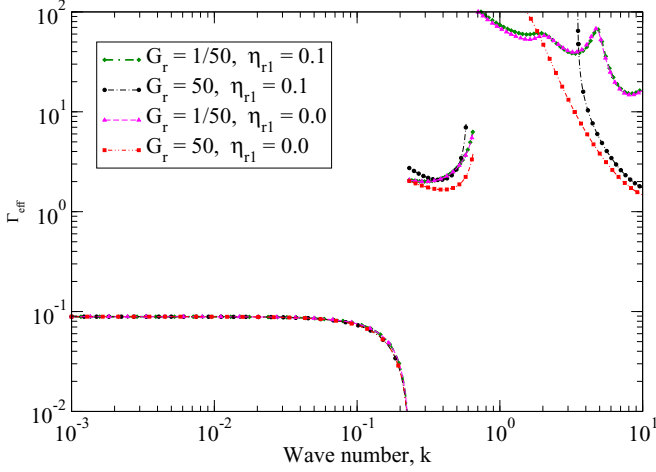


FIG. 10. Neutral stability curves for GL and LS modes of instability in the $\Gamma_{\text{eff}}-k$ plane: $G_r = 1/50$ and 50 , $\theta = \pi/4$, $\text{Re} = 1.0$, $H = 0.25$, $\beta = 0.5$, $\eta_{r2} = 0$, $\Sigma = 0$, $\Sigma_1 = 0$, $\Sigma_2 = 0$, and different η_{r1} values.

which was expected from asymptotic analysis. Interestingly, this increase only has a marginal stabilizing effect on the uppermost neutral stability curves. In contrast, when $G_r = 50$ (softer layer on top), the change in viscosity η_{r1} of the top layer now has a significant stabilizing effect on both of the upper neutral curves. Thus, an increase in the viscosity of the softer layer further increases the gap between the lower and upper neutral curves, and hence increases the region where mode 1 is completely suppressed. A similar trend is seen in Fig. 11, wherein the viscosity η_{r2} of the bottom solid layer is increased, and even here, only the increase in the viscosity of the softer layer has a significant stabilizing effect. This discussion thus shows that while the viscosity of either of the two solid layers does not have a destabilizing effect, the viscosity of the softer layer (regardless of its placement) has a substantial stabilizing impact on the upper neutral curves, and hence it increases the window of stability.

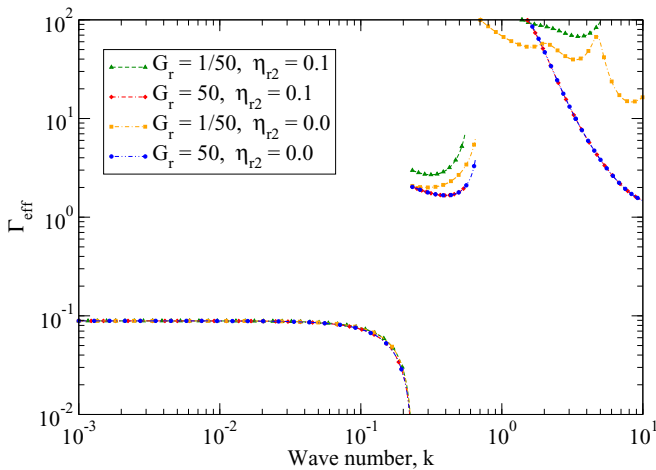


FIG. 11. Neutral stability curves for GL and LS modes of instability in the $\Gamma_{\text{eff}}-k$ plane: $G_r = 1/50$ and 50 , $\theta = \pi/4$, $\text{Re} = 1.0$, $H = 0.25$, $\beta = 0.5$, $\eta_{r1} = 0$, $\Sigma = 0$, $\Sigma_1 = 0$, $\Sigma_2 = 0$, and different η_{r2} values.

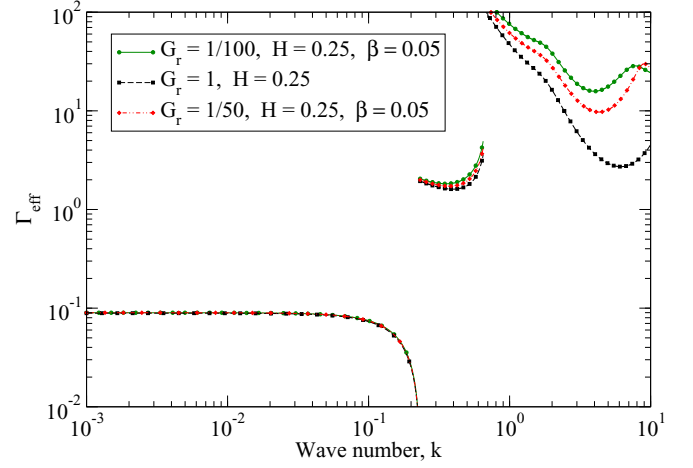


FIG. 12. Neutral stability curves for GL and LS modes of instability in the $\Gamma_{\text{eff}}-k$ plane: $G_r = 1/100$ and $1/50$, $\theta = \pi/4$, $\text{Re} = 1.0$, $H = 0.25$, $\beta = 0.05$, $\eta_{r1} = \eta_{r2} = 0$, and $\Sigma = \Sigma_1 = \Sigma_2 = 0$.

We next consider the case of a very thin hard layer of solid that is placed over a much thicker softer solid. Figure 12 shows that if the parameters are chosen carefully, the free-surface instability can be suppressed up to a large domain of Γ_{eff} . As G_r is decreased (at a fixed β , thickness of the top layer), we find the upper neutral curves to shift upward, indicating a strong stabilizing effect. This clearly demonstrates that the upper neutral curves are highly sensitive to the modulus of the solid layer adjacent to the fluid, while the lower neutral curve is independent of those changes, and is a function only of the effective modulus.

V. CONCLUSION

Previous studies have demonstrated that passive suppression of free-surface and interfacial instabilities (which otherwise exist in flow past rigid surfaces) is possible by considering a deformable solid layer lining over the rigid substrate in a variety of contexts. However, a major aspect of using a deformable solid layer is that new instabilities due to the deformability of the solid layer could potentially proliferate, and hence it is necessary to have an accurate understanding of the window in the parameter space in which free-surface and other deformability-induced instabilities are suppressed at all wave numbers. In the present study, we proposed and evaluated the possibility of using a deformable “bilayer” solid, in which two solid layers, of different physical properties (elastic moduli, viscosity, and thickness) are sandwiched together, for the specific case of suppression of the free-surface instability in flow down an inclined plane. Such a flow is known to become unstable in flow down a rigid incline, and a key feature of this instability is that the flow is unstable in the limit of long wavelengths. We carried out an asymptotic analysis in the long-wave limit for free-surface flow past a bilayer, which showed that the free-surface instability could indeed be suppressed in the long-wave limit, and the parameter that determines the suppression is the effective shear modulus of the bilayer, and not the individual shear moduli of the solid layers. Thus, our asymptotic analysis shows that the suppression of the instability is independent of the ordering

of the two solid layers in the bilayer. Interestingly, the recent work of Neelamegam *et al.* [26] showed that for single-layer plane Couette flow past a bilayer, the liquid-solid interfacial instability depends on the specific bilayer configuration. Even in the present case, as the solid is made sufficiently deformable, new instabilities (absent in flow down a rigid incline) appear, and these new instabilities do depend on the relative placement of the two solid layers.

The asymptotic result [Eq. (43)] can be used to provide some estimates on the values of physical parameters for which the present predictions could be realized in experiments. For a vertical plate, the asymptotic result predicts that $9\Gamma_{\text{eff}}H > \frac{6}{5}\text{Re}$ for suppression of instability, which in terms of dimensional parameters reduces to $G_{\text{eff}} < \frac{15}{2}\eta^2 H/\rho R^2$. Using $\eta \sim 10^{-1}$ Pa s, $\rho \sim 10^3$ kg/m³, $R \sim 10^{-4}$ m, and $H = 1/4$, we obtain $G_{\text{eff}} < 2000$ Pa. Upon using the expression for G_{eff} and $\beta = 0.05$, we obtain $G_1 \sim 10^5$ Pa and $G_2 \sim 10^3$ Pa. Thus, the present predictions are expected to be valid for the flow of highly viscous liquid layers (with viscosity $\sim 10^{-1}$ Pa s), of thickness in the range of 100 microns, with the shear modulus of the hard and soft layers in the range 10^5 and 10^3 Pa, respectively. We also carried out numerical computations at finite inertia and wave number to demonstrate that it is possible to choose the bilayer configuration (based on relative placement, elastic moduli, thickness, and viscosity) in such a manner that the window of parameters in which the system is stable to perturbations of all wavelengths can be significantly enhanced. Further, incorporation of dissipative effects in the solid showed that it is the viscosity of the softer solid that leads to a substantial increase in the stable window, and that the viscosity of the harder layer does not have a major impact on the stability. While this study has focused on the stability of flow down an inclined plane, we expect that the qualitative trends would carry over to more complicated flows such as two-layer or core-annular flows with two immiscible fluids. Thus, deformable solid bilayers offer significantly more options in the control and manipulation of interfacial instabilities in free-surface and multilayer flows.

APPENDIX A: WAVE SPEED FROM ASYMPTOTIC ANALYSIS

In the asymptotic analysis, the complex wave speed can be expanded in a series of k for $k \ll 1$. As discussed in Sec. III, it is sufficient to consider terms up to $O(k)$ correction to wave speed in the present study. Thus, the expansion of c leads to

$$c = c^{(0)} + kc^{(1)} + \dots \quad (\text{A1})$$

We consider small perturbations in the present study in which \tilde{v}_z could be assumed to be of $O(1)$, and using continuity equation (15) and x -momentum equation (16), we conclude $\tilde{v}_x \sim O(k^{-1})$ and $\tilde{p} \sim O(k^{-2})$, respectively. The expansion of the velocity and pressure in the liquid layer now are as follows:

$$\tilde{v}_z = \tilde{v}_z^{(0)} + k\tilde{v}_z^{(1)} + \dots, \quad (\text{A2})$$

$$\tilde{v}_x = k^{-1}\tilde{v}_x^{(0)} + \tilde{v}_x^{(1)} + \dots, \quad (\text{A3})$$

$$\tilde{p} = k^{-2}\tilde{p}^{(0)} + k^{-1}\tilde{p}^{(1)} + \dots \quad (\text{A4})$$

On a similar ground, the expansion of the dynamic quantities governing the dynamics of the upper solid layer, up to $O(k)$

consideration of u_{z1} , could be expanded as

$$\tilde{u}_{z1} = \tilde{u}_{z1}^{(0)} + k\tilde{u}_{z1}^{(1)} + \dots, \quad (\text{A5})$$

$$\tilde{u}_{x1} = k^{-1}\tilde{u}_{x1}^{(0)} + \tilde{u}_{x1}^{(1)} + \dots, \quad (\text{A6})$$

$$\tilde{p}_{g1} = k^{-2}\tilde{p}_{g1}^{(0)} + k^{-1}\tilde{p}_{g1}^{(1)} + \dots \quad (\text{A7})$$

Similarly, the displacements and pressure fields in the lower solid layer are expanded as follows:

$$\tilde{u}_{z2} = \tilde{u}_{z2}^{(0)} + k\tilde{u}_{z2}^{(1)} + \dots, \quad (\text{A8})$$

$$\tilde{u}_{x2} = k^{-1}\tilde{u}_{x2}^{(0)} + \tilde{u}_{x2}^{(1)} + \dots, \quad (\text{A9})$$

$$\tilde{p}_{g2} = k^{-2}\tilde{p}_{g2}^{(0)} + k^{-1}\tilde{p}_{g2}^{(1)} + \dots \quad (\text{A10})$$

Since the displacement fields in the solid layers are defined, the kinematic equation of the evolution of the free surface interface from Eq. (27) dictates that the coefficient of the free-surface height fluctuation can be expanded in a similar asymptotic series in k :

$$\tilde{h} = k^{-1}\tilde{h}^{(0)} + \tilde{h}^{(1)} + \dots \quad (\text{A11})$$

To obtain the governing linearized equation in the liquid and solid layers at the corresponding leading order and the first correction, we substitute the series expansion of the perturbed dynamical quantities into the linearized equations for liquid, Eqs. (15)–(18), and for the two solid layers, Eqs. (19)–(22) and Eqs. (23)–(26), respectively. Similarly, the boundary and the interface conditions at the leading order and $O(k)$ could be obtained from substituting the expansion into Eqs. (27)–(39). We further divide this appendix into two subparts that deal with the sequential procedure of the calculations of the leading-order and $O(k)$ dynamical quantities.

1. Leading-order dynamics

The governing equations for the leading-order velocity field $\tilde{v}_z^{(0)}$ in the liquid layer and the leading-order deformation fields $\tilde{u}_{z1}^{(0)}$ and $\tilde{u}_{z2}^{(0)}$ in the solid layers, as obtained from the asymptotic series expansion, are

$$d_z^4 \tilde{v}_z^{(0)} = 0, \quad (\text{A12})$$

$$d_z^4 \tilde{u}_{z1}^{(0)} = 0, \quad (\text{A13})$$

$$d_z^4 \tilde{u}_{z2}^{(0)} = 0. \quad (\text{A14})$$

The leading-order boundary conditions at the free-surface interface, $z = 0$, are

$$-3\tilde{h}^{(0)} + d_z \tilde{v}_x^{(0)} = 0, \quad (\text{A15})$$

$$-\tilde{p}^{(0)} = 0. \quad (\text{A16})$$

Similarly, the leading-order interface conditions at the fluid-solid interface, $z = 1$, are

$$\tilde{v}_z^{(0)} = 0, \quad (\text{A17})$$

$$\tilde{v}_x^{(0)} = 0, \quad (\text{A18})$$

$$d_z \tilde{v}_x^{(0)} = \frac{1}{\Gamma_1} d_z \tilde{u}_{x1}^{(0)}, \quad (\text{A19})$$

$$\tilde{p}^{(0)} = \tilde{p}_{g1}^{(0)}. \quad (\text{A20})$$

The interface conditions at the solid-solid interface at $z = (1 + \beta H)$ are

$$\tilde{u}_{z1}^{(0)} = \tilde{u}_{z2}^{(0)}, \quad (\text{A21})$$

$$\tilde{u}_{x1}^{(0)} = \tilde{u}_{x2}^{(0)}, \quad (\text{A22})$$

$$\frac{1}{\Gamma_1} d_z \tilde{u}_{x1}^{(0)} = \frac{1}{\Gamma_2} d_z \tilde{u}_{x2}^{(0)}, \quad (\text{A23})$$

$$\tilde{p}_{g1}^{(0)} = \tilde{p}_{g2}^{(0)}. \quad (\text{A24})$$

Lastly, the boundary conditions at $z = (1 + H)$ are

$$\tilde{u}_{z2}^{(0)} = 0, \quad \tilde{u}_{x2}^{(0)} = 0. \quad (\text{A25})$$

An important consequence of the low-wave-number expansion for the interface conditions [Eqs. (30) and (31)] is that leading order, the fluid velocities $\tilde{v}_z^{(0)}$ and $\tilde{v}_x^{(0)}$ satisfy the no-slip conditions at $z = 1$ as in a rigid boundary [Eqs. (A17) and (A18)]. This is because the right side of Eqs. (30) and (31) is $O(k)$ smaller than the fluid velocities on the left side. This implies that the solid-layer deformability does not influence the leading-order fluid velocity field, and so the leading-order wave speed in the present problem must be identical to that of Yih's [15] analysis. However, the leading-order velocity field in the liquid layer exerts a shear stress on the solid layer via the tangential stress condition [Eq. (A19)], and this causes a deformation in the solid layer at leading order. We now present the solution to the leading-order velocity and displacement fields, and the leading-order wave speed.

The analytical solution to the fourth-order differential equation (A12) is given as

$$\tilde{v}_z^{(0)} = A_1 + A_2 z + A_3 z^2 + A_4 z^3. \quad (\text{A26})$$

Since this ordinary differential equation (ODE) is linear and homogeneous in itself, the eigenfunction \tilde{v}_z obtained from it is determined only to a multiplicative constant. Therefore, $A_1 = 1$ could be chosen without any loss of generality. Physically, we can interpret this as the normalization of the amplitude of the normal component of the leading-order liquid velocity at the free surface by 1. The solutions to the leading-order dynamical variables of the liquid layer could be obtained by satisfying the leading-order boundary conditions [Eqs. (A16)–(A18)],

$$\tilde{v}_z^{(0)} = (z - 1)^2, \quad (\text{A27})$$

$$\tilde{v}_x^{(0)} = 2i(z - 1), \quad (\text{A28})$$

$$\tilde{p}^{(0)} = 0. \quad (\text{A29})$$

The free-surface height fluctuation at $z = 0$, to a leading order, could be found using Eq. (A16),

$$\tilde{h}^{(0)} = 2i/3. \quad (\text{A30})$$

Therefore, the leading-order wave speed could be found using the linearized kinematic condition (27), and it is given as

$$c^{(0)} = 3, \quad (\text{A31})$$

which matches Yih's [15] result for liquid flow down an inclined rigid plane, as expected. Since the flow is neutrally stable to leading order, the stability of the system would be determined from the first correction to the wave speed. We would also be requiring the leading-order deformation in both

of the solid layers, and this could be obtained by solving the differential equations (A13) and (A14), whose solutions are given as

$$\tilde{u}_{z1}^{(0)} = B_1 + B_2 z + B_3 z^2 + B_4 z^3, \quad (\text{A32})$$

$$\tilde{u}_{z2}^{(0)} = C_1 + C_2 z + C_3 z^2 + C_4 z^3. \quad (\text{A33})$$

The multiplicative constants in the above solutions could be determined using the boundary conditions [Eqs. (A19)–(A25)]. Finally, the leading-order deformation fields are given as

$$\tilde{u}_{z1}^{(0)} = \Gamma_1 \{z - (1 + \beta H)\}^2 \quad (\text{A34})$$

$$+ (1 - \beta)\Gamma_2 H \{2 + (1 + \beta)H - 2z\}, \quad (\text{A35})$$

$$\tilde{u}_{x1}^{(0)} = 2i[\Gamma_1 \{z - (1 + \beta H)\} - \Gamma_2 H(1 - \beta)], \quad (\text{A36})$$

$$\tilde{p}_{g1}^{(0)} = 0, \quad (\text{A37})$$

$$\tilde{u}_{z2}^{(0)} = \Gamma_2 [z - (1 + H)]^2, \quad (\text{A38})$$

$$\tilde{u}_{x2}^{(0)} = 2i\Gamma_2 [z - (1 + H)], \quad (\text{A39})$$

$$\tilde{p}_{g2}^{(0)} = 0. \quad (\text{A40})$$

With the calculation of the above leading-order dynamical quantities, we now proceed to evaluate the first correction to the wave speed $c^{(1)}$.

2. First correction to the wave speed

The $O(k)$ equation obtained for the velocity field \tilde{v}_z , which represents the dynamics of $\tilde{v}_z^{(1)}$, is

$$d_z^4 \tilde{v}_z^{(1)} = i \operatorname{Re}[(\tilde{v}_x - c^{(0)})d_z^2 \tilde{v}_z^{(0)} - (d_z^2 \tilde{v}_x) \tilde{v}_z^{(0)}]. \quad (\text{A41})$$

The general solution to this inhomogeneous fourth-order differential equation (A41) is given as

$$\tilde{v}_z^{(1)} = D_1 + D_2 z + D_3 z^2 + D_4 z^3 - \frac{i \operatorname{Re}}{20} z^5. \quad (\text{A42})$$

The multiplicative constant D_1 must be set to zero since previously we have fixed the amplitude of \tilde{v}_z at $z = 0$ to be 1 by setting the coefficient A_1 at the leading order to be 1. The boundary conditions at $z = 0$ and 1, Eqs. (27)–(30), are used to determine the remaining three constant coefficients. At the free-surface interface $z = 0$, the continuity conditions for tangential and normal stress equations at order $O(k)$ are

$$-3\tilde{h}^{(1)} + d_z \tilde{v}_x^{(1)} = 0, \quad (\text{A43})$$

$$-\tilde{p}^{(1)} - 3\tilde{h}^{(0)} \cot \beta = 0. \quad (\text{A44})$$

At the solid-liquid interface $z = 1$, the velocity continuity conditions at order $O(k)$ are

$$\tilde{v}_z^{(1)} = -ic^{(0)} \tilde{u}_{z1}^{(0)}, \quad (\text{A45})$$

$$\tilde{v}_x^{(1)} + d_z \tilde{v}_x|_{z=1} \tilde{u}_{z1}^{(0)} = -ic^{(0)} \tilde{u}_{x1}^{(0)}. \quad (\text{A46})$$

This coupling of liquid-solid at the interface gives rise to the $O(k)$ velocity perturbation field, which is solely affected by the leading-order deformation field in the upper solid layer. Using Eqs. (A44)–(A46), the $O(k)$ component of the perturbed velocity field is determined. The obtained solution for $\tilde{v}_z^{(1)}$ is

as follows:

$$\begin{aligned} \tilde{v}_z^{(1)} = & -\frac{iz}{60} \{3[60\beta^2(\Gamma_1 - \Gamma_2)H^2 + 60\Gamma_2H(2 + H - 2z) \\ & - 120\beta(\Gamma_1 - \Gamma_2)H(-1 + z) \\ & + \text{Re}(-1 + z)^2(-7 + 2z + z^2)] \\ & + 20(-1 + z)^2 \cot \beta\}. \end{aligned}$$

The inclusion of solid-layer deformation in the first correction is through the terms that are proportional to Γ_1 and Γ_2 . The first correction to the height fluctuation $\tilde{h}^{(1)}$ obtained from Eq. (A43) is

$$\tilde{h}^{(1)} = -4H[\Gamma_1\beta + \Gamma_2(1 - \beta)] + \frac{8}{15}\text{Re} - \frac{4}{9}\cot\beta. \quad (\text{A47})$$

Finally, the linearized kinematic condition, Eq. (27), to $O(k)$, given as

$$i[\tilde{v}_x|_{z=0} - c^{(0)}]\tilde{h}^{(1)} - ic^{(1)}\tilde{h}^{(0)} = \tilde{v}_z^{(1)}|_{z=0}, \quad (\text{A48})$$

is used to calculate the first correction to the wave speed $c^{(1)}$,

$$c^{(1)} = i\left[\left[\frac{6}{5}\text{Re} - \cot\beta\right] - 9H[\Gamma_1\beta + \Gamma_2(1 - \beta)]\right]. \quad (\text{A49})$$

APPENDIX B: CHARACTERISTIC EQUATION AT ARBITRARY WAVE NUMBERS

In this appendix, we illustrate the numerical technique used to solve the governing equations and boundary conditions described in Sec. II C. A shooting technique is implemented in which an initial guess of the solution (c , here) is provided, and with the help of the Newton-Raphson method, the final value of the iterated eigenvalue is obtained after following sufficient iterations so as to meet the suitable convergence criterion. This method of numerical integration is very common in the linear stability analysis, and therefore the solution methodology has been adopted from [12,13]. A brief explanation of the coding procedure is further explained here: The governing equations for the liquid and solid layers can be recast into respective single fourth-order ordinary differential equations (ODEs). Therefore, we have three fourth-order ODEs governing \tilde{v}_z for liquid and \tilde{u}_{z1} and \tilde{u}_{z2} in the solid layers. These three fourth-order ODEs along with boundary conditions completely specify the eigenvalue problem, the parameter c (complex

wave speed) being the eigenvalue. The numerical code for arbitrary Re uses the fourth-order Runge-Kutta integrator with a uniform step-size control to numerically integrate the ODEs, and a Newton-Raphson technique to find the solution of a characteristic equation. We first started from the lower solid layer and we began moving toward the free surface of the liquid layer. To carry this out, we must specify ‘‘initial conditions’’ for the function \tilde{u}_{z2} and its first three derivatives at a given value of the independent variable z . For the lower solid layer at $z = (1 + H)$, we have the zero displacement conditions $\tilde{u}_{z2} = 0$ and $\tilde{u}_{x2} = \frac{i}{k}d_z\tilde{u}_{z2} = 0$. We use two different (linearly independent) sets of higher derivatives, $d_z^2\tilde{u}_{z2} = (1,0)$ and $d_z^3\tilde{u}_{z2} = (0,1)$, at $z = (1 + H)$ and we numerically integrate the differential equation (26) up to $z = (1 + \beta H)$. This yields two linearly independent solutions to the displacement field consistent with the two zero displacement conditions at $z = (1 + H)$ in the solid layer. Corresponding to these two linearly independent solutions, we evaluate the displacement field of the upper solid layer \tilde{u}_{z1} and its higher derivatives [which will be acting as the initial guesses for the shooting method while integrating the fourth-order differential equation in the upper solid layer ranging from $z = (1 + \beta H)$ to $z = 1$] from the interfacial conditions at $z = (1 + \beta H)$ [Eqs. (34)–(37)]. Using these two sets of values of \tilde{u}_{z1} acting as initial guesses, we now numerically integrate the fourth-order differential equation (22) from $z = (1 + \beta H)$ to $z = 1$. After applying the interface conditions [Eqs. (30)–(33)], we obtain the velocity field \tilde{v}_z and its higher derivatives in the liquid layer at $z = 1$, which again will be acting as the initial guesses for integrating the fourth-order differential equation (18). Using these two sets of values for \tilde{v}_z and its derivatives as the initial guesses, we integrate the Orr-Sommerfeld equation (18) for the fluid starting from $z = 1$ to the free surface at $z = 0$. The velocity field in the fluid is obtained as a linear combination of these two solutions. At $z = 0$, the fluid velocity field must satisfy the free-surface conditions (28) and (29). This is written in matrix form, and the determinant of this matrix is set to zero to obtain the characteristic equation. This is solved numerically using a Newton-Raphson iteration procedure to obtain the eigenvalue c , for species values of Γ_{eff} , Re , k , β , H , Σ , Σ_1 , Σ_2 , η_{r1} , and η_{r2} . We use the low- k asymptotic results as a starting guess for the numerical procedure, and we continue with the low- k results numerically to finite values of k .

-
- [1] T. W. Kao, Role of viscosity stratification in the instability of two-layer flow down an incline, *J. Fluid Mech.* **33**, 561 (1968).
 [2] D. S. Loewenherz and C. J. Lawrence, The effect of viscosity stratification on the stability of a free surface flow at low Reynolds number, *Phys. Fluids A* **1**, 1686 (1989).
 [3] C. Pozrikidis, Instability of multilayer channel and film flows, *Adv. Appl. Mech.* **40**, 179 (2004).
 [4] K. P. Chen, The onset of elastically driven wavy motion in the flow of two viscoelastic liquid films down an inclined plane, *J. Non-Newtonian Fluid Mech* **45**, 21 (1992).
 [5] Y. Renardy, Stability of the interface in two-layer Couette flow of upper convected Maxwell liquids, *J. Non-Newtonian Fluid Mech.* **28**, 99 (1988).
 [6] K. P. Chen, Wave formation in the gravity-driven low-Reynolds number flow of two liquid films down an inclined plane, *Phys. Fluids A* **5**, 3038 (1993).
 [7] W. Y. Jiang, B. Helenbrook, and S. P. Lin, Inertialess instability of a two-layer liquid film flow, *Phys. Fluids* **16**, 652 (2004).
 [8] W. Y. Jiang and S. P. Lin, Enhancement or suppression of instability in a two-layered liquid film flow, *Phys. Fluids* **17**, 054105 (2005).
 [9] A. S. Utada *et al.*, Monodisperse double emulsions generated from a microcapillary device, *Science* **308**, 537 (2005).
 [10] A. S. Utada *et al.*, Dripping, jetting, drops, and wetting: The magic of microfluidics, *MRS Bull.* **32**, 702 (2007).

- [11] S. P. Lin, J. N. Chen, and D. R. Woods, Suppression of instability in a liquid film flow, *Phys. Fluids* **8**, 3247 (1996).
- [12] V. Shankar and L. Kumar, Stability of two-layer Newtonian plane Couette flow past a deformable solid layer, *Phys. Fluids* **16**, 4426 (2004).
- [13] V. Shankar and A. K. Sahu, Suppression of instability in liquid flow down an inclined plane by a deformable solid layer, *Phys. Rev. E* **73**, 016301 (2006).
- [14] A. Jain and V. Shankar, Instability suppression in viscoelastic film flows down an inclined plane lined with a deformable solid layer, *Phys. Rev. E* **76**, 046314 (2007).
- [15] C.-S. Yih, Stability of liquid flow down an inclined plane, *Phys. Fluids* **6**, 321 (1963).
- [16] C.-S. Yih, Instability due to viscosity stratification, *J. Fluid Mech.* **27**, 337 (1967).
- [17] V. Kumaran, G. H. Fredrickson, and P. Pincus, Flow induced instability of the interface between a fluid and a gel at low Reynolds number, *J. Phys. II* **4**, 893 (1994).
- [18] L. Landau and E. Lifshitz, *Theory of Elasticity* (Pergamon, New York, 1989).
- [19] V. Gkanis and S. Kumar, Instability of creeping Couette flow past a neo-Hookean solid, *Phys. Fluids* **15**, 2864 (2003).
- [20] V. Gkanis and S. Kumar, Stability of pressure-driven creeping flows in channels lined with a nonlinear elastic solid, *J. Fluid Mech.* **524**, 357 (2005).
- [21] L. E. Malvern, *Introduction to the Mechanics of a Continuous Medium* (Prentice-Hall, Englewood Cliffs, NJ, 1969).
- [22] G. A. Holzapfel, *Nonlinear Solid Mechanics* (Wiley, Chichester, UK, 2000).
- [23] V. Gkanis and S. Kumar, Instability of gravity-driven free-surface flow past a deformable elastic solid, *Phys. Fluids* **18**, 044103 (2006).
- [24] Gaurav and V. Shankar, Stability of gravity-driven free-surface flow past a deformable solid layer at zero and finite Reynolds number, *Phys. Fluids* **19**, 024105 (2007).
- [25] V. Gkanis and S. Kumar, Instability of creeping flow past a deformable wall: The role of depth-dependent modulus, *Phys. Rev. E* **73**, 026307 (2006).
- [26] R. Neelmegam, D. Giribabu, and V. Shankar, Instability of viscous flow over a deformable two-layered gel: Experiment and theory, *Phys. Rev. E* **90**, 043004 (2014).